A mutation in the *Arabidopsis* γ-tubulin-containing complex causes helical growth and abnormal microtubule branching

Masayoshi Nakamura and Takashi Hashimoto*

Graduate School of Biological Sciences, Nara Institute of Science and Technology, Ikoma, Nara 630-0192, Japan

*Author for correspondence (e-mail: hasimoto@bs.naist.jp)

Accepted 10 March 2009
Journal of Cell Science 122, 2208-2217 Published by The Company of Biologists 2009
doi:10.1242/jcs.044131

Summary

Plant cortical microtubules are mainly nucleated on previously established microtubules, grow at a narrow range of angles to the wall of mother microtubules, and eventually are released from the nucleation sites. These nucleation events are thought to be regulated by γ-tubulin-containing complexes. We here show that a null mutation of *Arabidopsis* GCP2, a core subunit of the γ-tubulin-containing complex, severely impaired the development of male and female gametophytes. However, a missense mutation in the conserved grip1 motif, called *spiral3*, caused a left-handed helical organization of cortical microtubule arrays, and severe right-handed helical growth. The *spiral3* mutation compromises interaction between GCP2 and GCP3, another subunit of the complex, in yeast. In the *spiral3* mutant, microtubule dynamics and nucleation efficiency were not markedly affected, but nucleating angles were wider and more divergently distributed. A *spiral3 katanin* double mutant had swollen and twisted epidermal cells, and showed that the microtubule minus ends were not released from the nucleation sites, although the nucleating angles distributed in a similar manner to those in *spiral3*. These results show that *Arabidopsis* GCP2 has an important role in precisely positioning the γ-tubulin-containing complex on pre-existing microtubules and in the proper organization of cortical arrays.

Supplementary material available online at
http://jcs.biologists.org/cgi/content/full/122/13/2208/DC1

Key words: *Arabidopsis thaliana*, γ-tubulin-containing complex, Microtubule nucleation, GCP2, Twisting

Introduction

Although microtubule polymers can assemble in vitro from purified tubulins under appropriate conditions, eukaryotic cells tightly control the formation of new microtubules (termed 'nucleation') temporally and spatially. γ-Tubulin, a member of the tubulin family, and its associated proteins have dominant roles in microtubule nucleation and spindle assembly in evolutionally distant eukaryotic species (Wiese and Zheng, 2006). In fungal and animal cells, γ-tubulin is found in complexes with additional proteins, termed γ-tubulin complex proteins (GCPs). The γ-tubulin small complex (γ-TuSC) is a core nucleation unit composed of two molecules of γ-tubulin associated with one molecule each of GCP2 and GCP3. Animal cells also contain a larger complex called the γ-tubulin ring complex, which contains additional proteins, including GCP4, GCP5 and GCP6, and shows high nucleation activity in vitro, whereas different sets of proteins are associated with larger γ-tubulin complexes in yeasts (Wiese and Zheng, 2006).

The organization of non-centrosomal microtubule arrays in higher plants involves numerous nucleation sites dispersed on the cell cortex (Chan et al., 2003), on the nuclear surface (Erhardt et al., 2002), and possibly on spindles and other endomembranes (Shimamura et al., 2004). Although γ-tubulin is essential for the nucleation of plant microtubules (Murata et al., 2005; Binarová et al., 2006; Pastuglita et al., 2006), the nature of γ-tubulin-containing complexes and how they are recruited to individual nucleation sites are not known. In *Arabidopsis*, tandem affinity purification of γ-tubulin-associated proteins recovered GCP2 and GCP3, indicating that they are in the same complexes in vivo (Seltzer et al., 2007). Sequenced genomes of higher plants contain homologs of other accessory GCP proteins found in animal γ-tubulin ring complexes (e.g. Pastuglia and Bouchez, 2007), implying that the fundamental organization of plant nucleation complexes is similar to that in animal cells.

Cortical microtubules in interphase plant cells are predominantly nucleated from the γ-tubulin-containing sites on the lattices of previously established microtubules (Murata et al., 2005). A notable feature of the microtubule-dependent nucleation is that the branching angle between the mother microtubule and the newly formed daughter microtubule is well defined with an average of around 40°. Assembly of nascent microtubules at acute angles to the pre-existing microtubules was also observed in algal cells after depolymerization of cortical microtubules by oryzalin (Wasteneys and Williamson, 1989). The minus-end of daughter microtubules is eventually released from the nucleation site (Shaw et al., 2003; Murata et al., 2005), perhaps by the severing activities of katanin (Burk and Ye, 2002). Free microtubules then migrate on the cell cortex by a hybrid treadmilling mechanism (Shaw et al., 2003), interact with each other with outcomes of selective stabilization or depolymerization, and finally generate a particular array pattern (Dixit and Cyr, 2004). In rapidly elongating cells, such as the epidermal cells in the growth zones of the root or the etiolated hypocotyl, for example, single and bundled microtubules align approximately transversely to the cell's main axis of growth. Cortical microtubules, particularly the bundled microtubules, might guide the movement of cellulose synthase complexes through the plasma membrane, thereby playing crucial roles in determining the

ordered deposition of load-bearing cellulose microfibrils and anisotropic cell expansion (Paradez et al., 2006; Lucas and Shaw, 2008).

It is largely unknown how the microtubules are organized into specific array patterns (Ehrhardt and Shaw, 2006). Genetic screening recovered dozens of *Arabidopsis* twisting mutants that possess either right- or left-handed helical arrays of cortical microtubules in rapidly elongating cells (Ishida et al., 2007b; Perrin et al., 2007; Korolev et al., 2007). These twisting mutants are caused by mutations or overexpression of α- or β-tubulin, microtubule-associated proteins, and a mitogen-activated protein kinase phosphatase-like protein. Although exactly how the otherwise transverse microtubule array is transformed into helical microtubule arrays in mutant cells has yet to be clarified, microtubule stability and microtubule dynamics at either plus- or minus-ends are proposed to be important for the proper organization of cortical arrays (Ishida et al., 2007a; Yao et al., 2008).

In this paper, we report that a partial loss-of-function mutation of *Arabidopsis* GCP2 generates a left-handed helical array of cortical microtubules and right-handed helical growth. Interestingly, the branching angle of microtubule nucleation is less tightly controlled in the mutant, providing evidence of a role for GCP2 in the positioning of γ-tubulin-containing nucleating complexes on the wall of pre-existing microtubules.

Results

Anisotropic cell expansion is impaired in the right-handed twisting mutant *spr3*

In our continued screening for twisting mutants of *Arabidopsis thaliana*, we isolated a novel right-handed helical growth mutant, designated *spiral3* (*spr3*). This mutant was generated in the Wassilewskija ecotype, and is caused by a recessive single-locus mutation (data not shown). The *spr3* plants grew normally and were fertile, but several microtubule-dependent morphological characteristics were altered compared with wild-type plants (Fig. 1). When *Arabidopsis* seedlings were grown on a hard agar plate, wild-type roots grew downward in the direction of the gravity vector, whereas *spr3* roots sharply skewed to the right side of the plate when viewed in front of the plate. A pair of wild-type cotyledons extended in a straight line in opposite directions, whereas *spr3* cotyledons twisted in a counterclockwise direction when viewed from above. Similar counterclockwise twisting was observed in *spr3* petals but not in wild-type petals. At the cell level, epidermal cell files of etiolated hypocotyls and roots were straight along the main axis of the organs in the wild type, but formed right-handed helices in the *spr3* mutant.

In addition to having twisting elongating axial organs, *spr3* plants were impaired in cell morphogenesis of trichomes and pavement cells. Trichomes on the 14-day-old wild-type true leaves (n=389) had mainly three branches (63.5%) or two branches (35.5%). By contrast, trichomes on *spr3* leaves (n=419) mostly contained two branches (95.9%); three branched trichomes were scarce (0.4%) and needle-like trichomes with no branching point were also observed (3.6%). Reduced trichome branching has been reported in tubulin mutants (Abe et al., 2004) and in wild-type seedlings treated with microtubule-disrupting drugs (Mathur and Chua, 2000).

Arabidopsis leaf pavement cells develop from slightly elongated polygons (stage I) to stage II cells with multiple shallow lobes alternating with indentations or necks (Fu et al., 2002). Wild-type leaf pavement cells of late stage II show a characteristic jigsaw puzzle appearance with interdigitating lobes and indentations, whereas lobe outgrowth was reduced in the *spr3* mutant (see Fig. 1G). The complexity of cell shapes was estimated by using circularity values (Le et al., 2006), where 1.0 ($4\pi\times$area/perimeter^2) indicates a perfect circle and an increasingly elongated polygon provides a smaller value. The circularity values for the wild-type

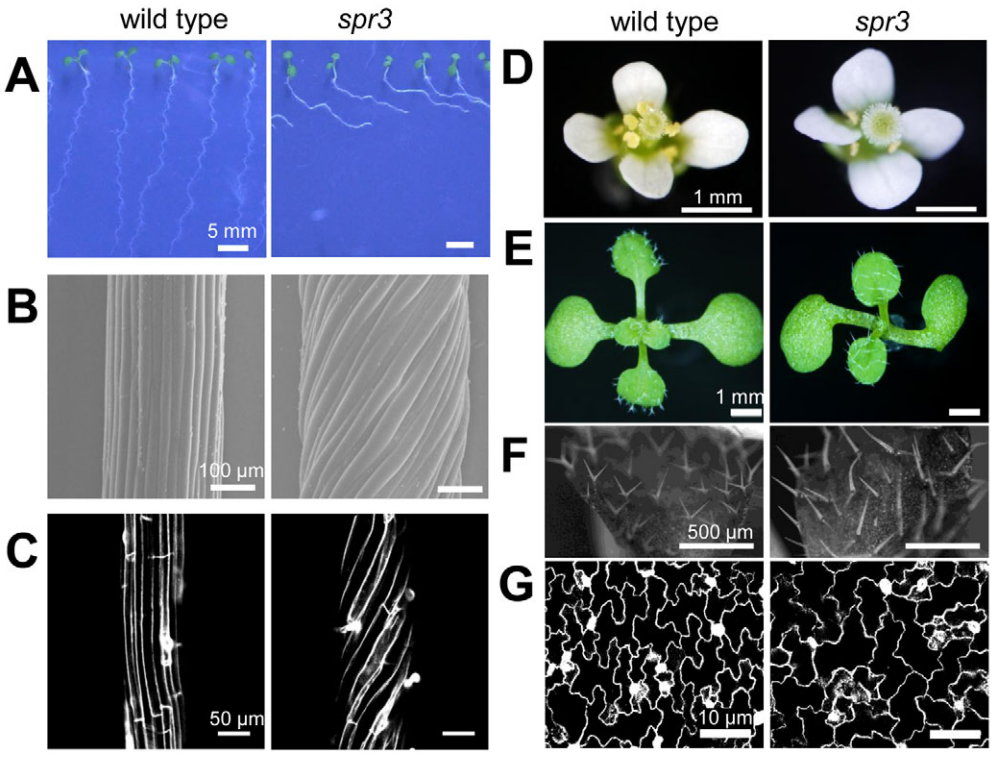

Fig. 1. Growth and cell morphology of *spr3*. Wild-type plants are shown on the left, whereas *spr3* plants are shown on the right. (A) 7-day-old seedlings grown on vertical hard agar plates. (B) Epidermal cell files of 4-day-old etiolated hypocotyls. Images obtained by scanning electron microscopy are shown. (C) Epidermal cell files of primary roots stained with propidium iodide. (D) Flowers of 3- to 4-week-old plants. (E) 10-day-old seedlings. (F) Leaf trichomes of first true leaves. (G) Pavement cells of third true leaves. Pavement cells of GFP-TUB6-expressing plants were optically sectioned by confocal microscopy at their median regions so that their contours were highlighted.

pavement cells (n=35) and the *spr3* cells (n=41) were 0.16±0.03 and 0.38±0.07, respectively, indicating that the *spr3* pavement cells are less interdigitated than the wild-type cells (P<0.01; Student's t-test).

Cortical microtubule organization in *spr3*

Since defects in mutant cell morphogenesis indicate a link between microtubule organization and SPR3 function, we analyzed the organization of cortical microtubule array. When root epidermal cells were analyzed by immunohistochemistry with an anti-tubulin antibody, it was found that the cortical microtubule arrays in the wild-type roots were mostly aligned transverse to the long axis of the cells, whereas those in the *spr3* roots were arranged in left-handed helices (Fig. 2A). Quantitative analysis of individual microtubule orientations showed that the *spr3* microtubules were skewed by ~11° on average in the direction of the left-handed helix relative to the wild-type distribution (Fig. 2B).

The microtubule organization in pavement cells was visualized in a microtubule marker line expressing GFP-β-tubulin-6 [GFP-TUB6 (Nakamura et al., 2004)]. In the late stage II control cells in which a jigsaw puzzle appearance was established, transversely ordered cortical microtubules were restricted to the neck region (Fu et al., 2002). By contrast, abundant and thick transverse cortical microtubules were found throughout the *spr3* cells (Fig. 2C).

The *spr3* mutant results from an amino-acid-exchange mutation in GCP2

We cloned the *SPR3* gene by a map-based cloning approach (supplementary material Fig. S1). The *SPR3* locus was mapped to a 30-kb interval on chromosome 5, in which seven genes were predicted to exist. After sequencing these candidate genes, we found a Gly-to-Arg substitution in the tenth exon of At5g17410, which encodes a subunit of the γ-tubulin-complex, GCP2 (Fig. 3A). The mutation changes the invariant Gly305 residue to Arg in the conserved Grip motif 1 (Fig. 3B). When an 8.7-kb region of the wild-type *GCP2* gene was introduced into the *spr3* mutant, all the anisotropic growth phenotypes, including the twisting growth, were complemented (Fig. 3C). Therefore, we conclude that the Gly305-to-Arg mutation in GCP2 causes the *spr3* phenotypes.

To examine the biochemical consequences of the *spr3* mutation, we assayed the interaction of GCP2 with GCP3, another subunit of the γ-tubulin-containing core complex, with a yeast two-hybrid system (Fig. 3D). When wild-type GCP2 protein fused to the Gal4 DNA-binding domain and a GCP3 protein fused to the Gal4 transcription-activating domain were expressed in the nucleus, they enabled growth of yeast cells on the selective medium and reconstituted the β-galactosidase activity. By contrast, a combination of the *spr3*-type G305R GCP2 mutant and wild-type GCP3 gave poor growth on the selective medium and highly reduced activity of β-galactosidase. Thus, the G305R mutation in GCP2 considerably compromises its interaction with GCP3 in yeast.

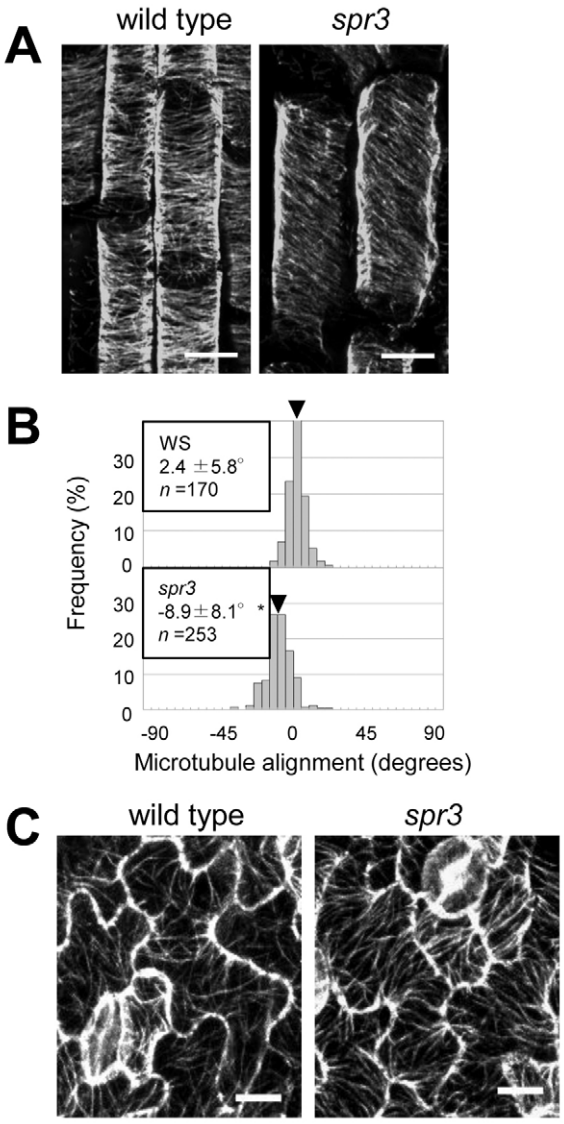

Fig. 2. Organization of cortical microtubules in *spr3* cells. (A) Cortical microtubule arrays in the epidermal cells of the elongation zone of 4-day-old seedling roots. Microtubules were fluorescently labeled by immunohistochemistry using anti-α-tubulin antibody. (B) Frequency distribution histograms of microtubule orientations in the root cells as shown in A. A left-handed helical organization of the microtubules gives negative values. The average angles (±s.d.) are shown and indicated with arrowheads above the histogram bars. The number of microtubules analyzed (n) is also shown. The asterisk indicates a statistically significant difference from the wild-type distribution (Student's t-test; P<0.05). (C) Cortical microtubules in pavement cells at late stage II from the third true leaves. Microtubules were visualized by expression of GFP-TUB6. Scale bars: 10 μm in A and C.

Microtubule nucleation frequency and microtubule dynamics are not strongly affected in *spr3* cells

Since abnormalities in microtubule nucleation were suspected in plants with the *spr3* allele of the GCP2 mutant, we compared the nucleation frequency of cortical microtubules in wild-type and *spr3* plants, in which microtubules were visualized using the GFP-TUB6 marker (Fig. 4A). The GFP-TUB6-expressing *Arabidopsis* plants do not show any morphological abnormalities (Abe and Hashimoto, 2005). The frequency of nucleation was evaluated in two independent experiments (Fig. 4B). In the first experiment, microtubule nucleation events were monitored in arbitrary regions (400 μm^2) of hypocotyl epidermal cells for 4 minutes. The microtubule nucleation frequency (approximately 1.3 events per minute per 400 μm^2) did not differ significantly between the control cells and the *spr3* cells. In the second experiment, nucleation events were counted along the length of preexisting cortical microtubules in hypocotyl epidermal cells, because cortical microtubule density might influence nucleation frequency. The calculated frequency

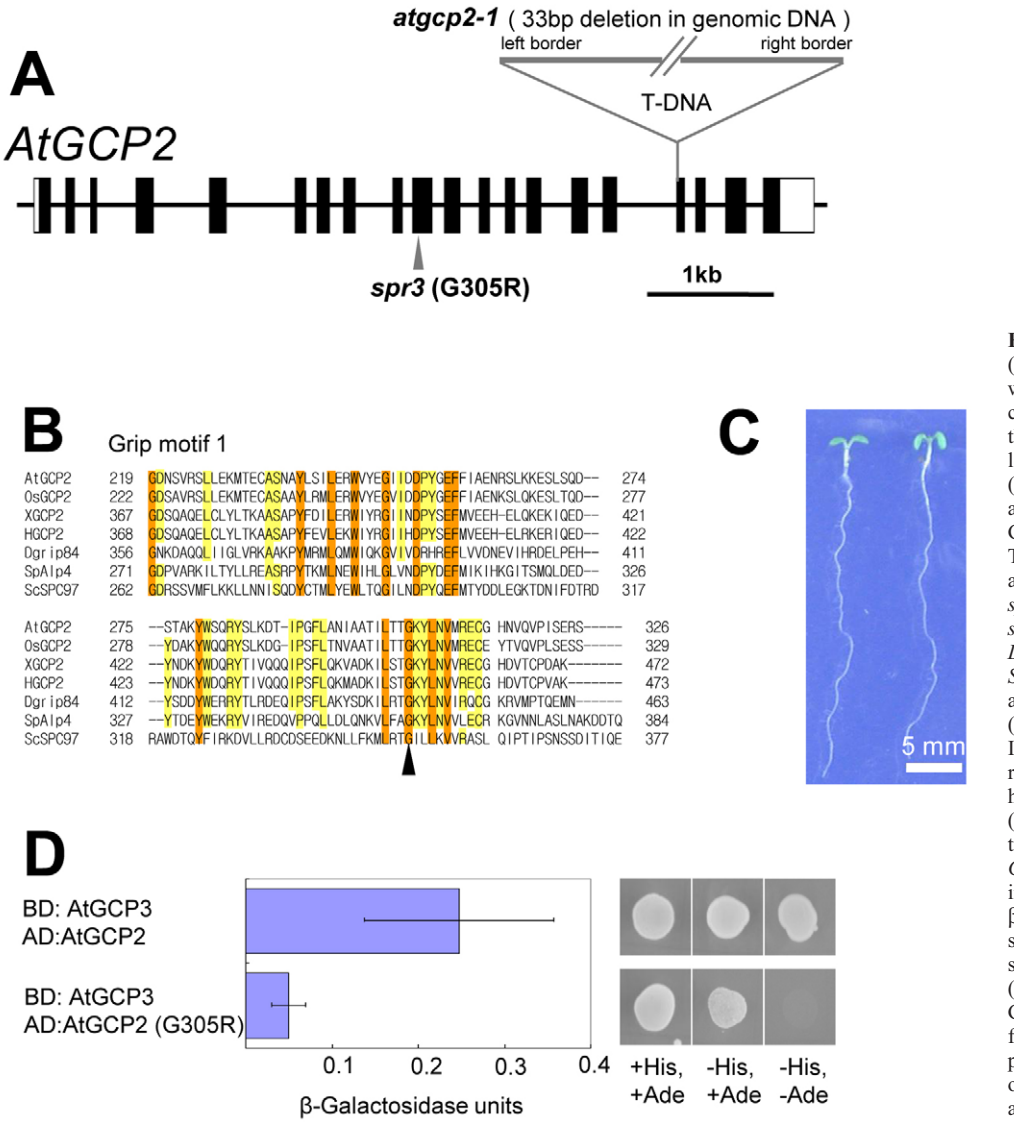

Fig. 3. The *spr3* locus encodes *GCP2*. (A) Genomic structure of *GCP2*. Black and white boxes represent coding and non-coding exons, respectively. Also shown are the T-DNA insertion site in *gcp2-1* and the location of the *spr3* missense mutation (G305R). (B) Amino acid sequence alignment of the Grip motif 1 in various GCP2 orthologs (Gunawardane et al., 2000). The conserved Gly305 (indicated with an arrowhead) was substituted with Arg in *spr3*. At, *Arabidopsis thaliana*; Os, *Oryza sativa*; X, *Xenopus*; H, human; D, *Drosophila*; Sp, *Saccharomyces pombe*; Sc, *Saccharomyces cerevisiae*. Sequences were aligned using the ClustalW program (http://clustalw.ddbj.nig.ac.jp/top-j.html). Invariant residues are boxed in orange, and residues conserved in five or six GCP homologs in the list are indicated in yellow. (C) 7-day-old *spr3* seedlings that had been transformed with a genomic region of *GCP2*. (D) Yeast two-hybrid analysis of interactions between GCP2 and GCP3. β-galactosidase activity was measured in seven independent clones by using the yeast semi-quantitative *ONPG* assay kit (Clontech). BD, construct fused to the GAL4 DNA-binding domain; AD, construct fused to the GAL4-activating domain. Right panels represent the growth of yeast clones on medium with or without histidine (His) and adenine (Ade).

values (approximately 0.002 events per minute per μm of microtubule) were indistinguishable between the control and *spr3*. Therefore, we conclude that microtubule nucleation efficiency was not measurably affected in the hypocotyl epidermal cells of *spr3* plants under standard growth conditions.

Next, we extended our analysis to microtubule dynamics by using the GFP-TUB6 marker. Parameters of dynamic instability for cortical microtubules were obtained in hypocotyl epidermal cells of a control line (the marker line), *spr3*, and a complemented transgenic line (*GCP2*/*spr3*) in which the wild-type *GCP2* gene was introduced into *spr3*. Table 1 shows rates of microtubule growth and shrinkage, frequencies of microtubule catastrophe and rescue, and percentages of time microtubules spent in periods of growth, pause or shrinkage. At the leading (plus) end of microtubules, these dynamic parameters were not significantly different between the control and *spr3* mutant and between *GCP2*/*spr3* and *spr3*, except that the growth rate in *spr3* plants was reduced by 19-20% compared with that in the control or *GCP2*/*spr3*. The biological consequences of this small but statistically significant difference are not clear. At the lagging (minus) end, the rescue frequency of *spr3* microtubules (0.119±0.090 events/second) was moderately but significantly ($P<0.01$; *t*-test) increased compared with the control value (0.058±0.050 events/second) and the value for *GCP2*/*spr3* (0.077±0.054 events/second), whereas microtubule minus-ends of *spr3* tended to spend more time in pause and less time in shrinkage, compared with minus-ends of control and *GCP2*/*spr3*. Other parameters at the minus-end were indistinguishable among the three types of cells. In summary, microtubule dynamics was not markedly affected by the *spr3* mutation, although depolymerizing minus ends of *spr3* microtubules stopped shrinking somewhat more frequently than those of control and reference microtubules.

Microtubule nucleating angles were shifted and more divergent in *spr3* cells

After careful observation of microtubule nucleation events, we noticed that the tight control of microtubule nucleating angles was compromised in the *spr3* cells. In GFP-TUB6-expressing control epidermal cells of hypocotyls and cotyledons, most cortical microtubules grew from the sides of other microtubules at a narrow range of angles, averaging approximately 40° to the wall of the existing microtubule (Fig. 4C). In the *spr3* cells, microtubule-nucleating angles distributed more widely, as evidenced by the larger

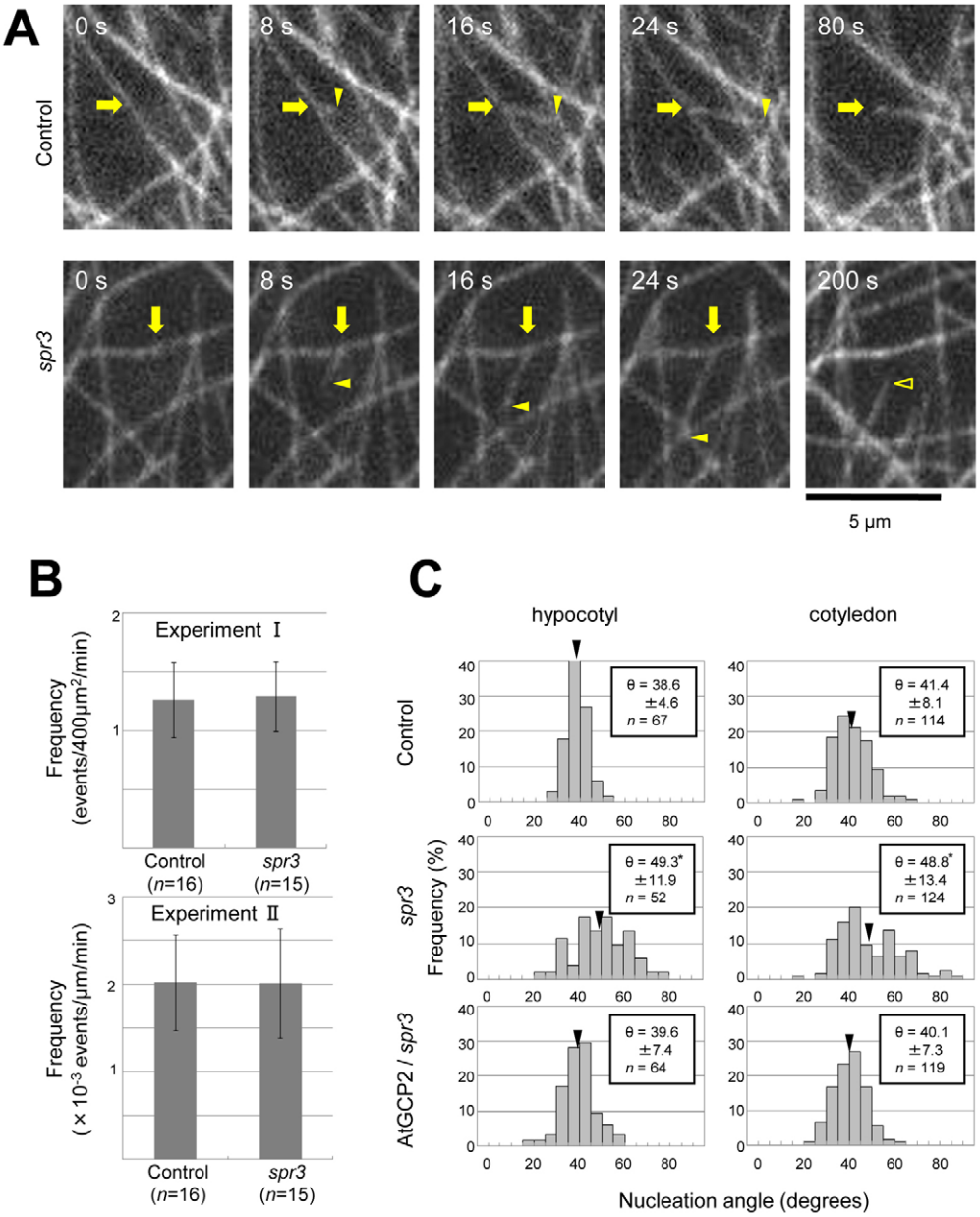

Fig. 4. Microtubule nucleation in *spr3* cells. (A) Cortical microtubules labeled with GFP-TUB6 were observed in cotyledon pavement cells by confocal microscopy. Representative nucleation events in control and *spr3* cells are shown. Nucleation sites are shown by arrows and the growing plus-ends of newly formed microtubules are indicated by filled arrowheads. In the control panels, the mother microtubule depolymerized and disappeared within 80 seconds. The minus end (open arrowhead) of the daughter microtubule in this *spr3* cell detached from the nucleation site within 200 seconds. Microtubule-branching angles in these particular episodes were 38° in the control and 56° in *spr3*. (B) Efficiency of microtubule nucleation in hypocotyl epidermal cells. In the first experiment, microtubule nucleation events were counted in the arbitrary cortical area of 400 μm^2. In the second, nucleation events were counted as a function of microtubule length. (C) Frequency distribution of microtubule-nucleating angles. Cotyledon pavement cells and hypocotyl epidermal cells of the control, *spr3* and GCP2-*spr3* (a *spr3* transgenic line complemented with a wild-type GCP2 genomic region) were analyzed. Averages of nucleating angles (±s.d.) are shown. Asterisks represent a statistically significant difference from both the control and GCP2-*spr3* (Student's *t*-test; $P<0.05$).

s.d. values, and the average nucleating angles increased by 7-10°, compared with those in the control. When the *spr3* phenotypes of twisting morphology and a skewed microtubule organization were rescued by introducing the wild-type *GCP2* gene, the distribution of microtubule-nucleating angles returned to the patterns observed for control cells, thereby confirming that the *spr3* mutation is responsible for the relaxed and altered distribution of the microtubule-nucleating angles.

Minus-end dynamics of *spr3* microtubules is not important for generating helical growth

The above observations identified two abnormalities in microtubule behavior of the *spr3* cells; slightly less dynamic minus-ends and less tight regulation of microtubule-nucleating angles. To assess the importance of dynamic minus-ends, we examined the morphological and cellular phenotypes of the *katanin spr3* double mutant. The *katanin* allele used had a mutation in the 60 kDa ATPase catalytic subunit of the heterodimeric katanin (McNally and Vale, 1993), which severs microtubules and might be responsible for the release of nascent microtubules from the cortical nucleation sites in plant interphase cells (Burk et al., 2001; Wasteneys, 2002). In the *katanin* single mutant, all types of interphase cells, except for tip-growing cells, exhibited a dramatic reduction in length and an increase in width, as shown for the epidermal cells of etiolated hypocotyls and roots in Fig. 5A. The epidermal cells of *katanin spr3* were short and swollen, and formed right-handed helical cell files; the additive cell morphology of *katanin* and *spr3*.

Immunostaining with an anti-tubulin antibody showed that, in *katanin* and the double mutant, cortical microtubule arrays of elongating root epidermal cells were organized aberrantly, and most microtubules were oriented in various angles with a wide deviation from the transverse direction (Fig. 5B,C). Many cortical microtubules converged at common sites, in an aster-like organization. A similar organization of cortical microtubules has

Table 1. Effects of *spr3* mutation on parameters of microtubule dynamic instability in the GFP-TUB6 transgenic background

Dynamic parameters	Wild type (*n*=72)	*spr3* (*n*=59)	Genomic GCP2/*spr3*[†] (*n*=61)
Leading end			
Growth rate (μm/minute)	5.85±2.91	4.68±2.56[§]	5.77±3.06
Shrinkage rate (μm/minute)	12.00±10.07	12.25±12.41	10.35±9.92
Catastrophe frequency (events/second)	0.019±0.013	0.020±0.014	0.022±0.014
Rescue frequency (events/second)	0.073±0.061	0.105±0.078	0.077±0.057
Time in growth phase	77.2%	75.2%	73.7%
Time in pause phase	7.5%	10.0%	10.5%
Time in shrinkage phase	15.4%	14.8%	15.8%
Lagging end			
Growth rate (μm/minute)	1.20±0.18	1.48±0.54	2.00±1.01
Shrinkage rate (μm/minute)	4.72±5.22	4.83±5.77	3.72±5.42
Catastrophe frequency (events/second)	0.208±0.072	0.188±0.068	0.236±0.041
Rescue frequency (events/second)	0.058±0.050	0.119±0.090[§]	0.077±0.054
Time in growth phase	0.1%	1.4%	0.5%
Time in pause phase	67.4%	80.4%	76.3%
Time in shrinkage phase	32.4%	18.2%	23.3%

Values are means ± s.d.
[†]Genomic GCP2/*spr3* represents plants in which *spr3* phenotypes are rescued by GCP2 genomic region constructs.
[§]Statistically significant difference from both wild-type plants and Genomic GCP2/*spr3* plants (Student's *t*-test; $P<0.01$).

been reported for various cell types with other *katanin* alleles (Bichet et al., 2001; Burk et al., 2001; Burk and Ye, 2002; Bouquin et al., 2003). It was noted that a minority of the epidermal cells with the *katanin* mutation had mostly aligned arrays, which were oriented in the transverse direction in *katanin* [as reported by Burk and Ye (Burk and Ye, 2002)] and shifted slightly in the left-handed helical direction in *katanin spr3*.

Time-lapse analysis of the microtubule nucleation events revealed that the minus-ends of cortical microtubules were not released from the nucleation sites on the wall of preexisting microtubules in the GFP-TUB6-expressing cells of *katanin* (Fig. 5D) and *katanin spr3* (not shown), indicating that the microtubule-severing activity of katanin is necessary for the microtubule release. Distribution patterns of microtubule nucleating angles in the epidermal cells of hypocotyls and cotyledons were indistinguishable between the control (Fig. 4C) and *katanin* (Fig. 5E). By contrast, nucleating angles in the double mutant cells were distributed more broadly and shifted to elevated values (Fig. 5E), as observed in the *spr3* single mutant cells (Fig. 4C). These results show that katanin is not involved in specifying the nucleating angles of nascent microtubules.

In conclusion, the observed mild defect in the minus-end microtubule dynamics is not essential to generate the helical growth in the *spr3* plants.

T-DNA knockout of GCP2 appears to cause embryonic lethality

Since *spr3* does not appear to be a fully non-functional allele, we searched the publicly available T-DNA or transposon insertion databases for insertion alleles of GCP2. In the *gcp2-1* allele (Wassilewskija ecotype), a single T-DNA was inserted after the first nucleotide G of the 17th exon and an accompanying 33-bp deletion removed after the insertion site (Fig. 3A). The heterozygous *gcp2-1* plants were indistinguishable from wild-type plants, but we could not recover homozygous plants from the selfed progeny of the heterozygous plants. The siliques of self-pollinated *gcp2-1* heterozygous plants contained desiccated ovules and aborted seeds (Fig. 6A), thereby reducing the number of fully developed seeds in a silique to approximately 40% of that in the self-pollinated wild-type plants (Fig. 6B). When an 8.7-kb genomic region of the wild-type *GCP2* gene was introduced, we could obtain transgenic plant lines that were homozygous for the *gcp2-1* allele, which grew normally and set seeds at the wild-type level (Fig. 6B). Therefore, we conclude that the null allele of GCP2 does not produce viable seeds, and that *spr3* is a partial loss-of-function allele.

T-DNA-knockout allele of GCP2 is defective in gametophyte development

A high percentage of undeveloped ovules indicates that gametophyte functions might be impaired in *gcp2-1*. To analyze the transmission efficiency of female and male *gcp2-1* gametes, we used heterozygous plants in reciprocal crosses with wild-type plants. When wild-type pollen was pollinated on heterozygous *gcp2-1* pistils, only 3.4% of the progeny plants (n=143) carried the *gcp2-1* mutant allele, instead of the 50% expected for full transmission. When pollen of *gcp2-1* heterozygous plants was used for the cross to wild-type plants, the *gcp2-1* mutant allele was recovered in 17% of the progeny (n=205). Therefore, the transmission of mutant gametes was reduced by 93% on the female side and by 66% on the male side, showing that the *gcp2-1* mutation drastically affects the development and function of both male and female haploid gametophytes.

We thus examined mature ovules by confocal microscopy according to the procedure used to visualize the embryo sac (Fig. 6C) (Christensen et al., 1997). Less than 1% of ovules had abnormal gametophytes (n=127) in wild-type plants. By contrast, abnormal gametophytes with reduced numbers of nuclei were found in 38% of mature ovules (n=426) in pistils of *gcp2-1*/+ plants. Synergids nucleoli were frequently absent and a large vacant space was generally found in the micropylar region of the abnormal female gametophytes.

To directly compare the development of *gcp2-1* and wild-type male gametophytes, we used the *quartet* (*qrt*) mutant, which produces four microspores that remain associated as a tetrad (Preuss et al., 1994). At the mature stage, more than 99% of the *qrt* tetrads contained four pollen grains, which possess a tricelled structure containing two sperm cells enclosed in a vegetative cell (Fig. 6D). In the *qrt*/*qrt*; *gcp2-1*/+ plants, however, 69% of the tetrads (n=146) contained one or two abnormal pollen grains, in which 22% of the tetrads had a bicellular pollen grain with one large sperm cell nucleus, 40% had one aborted microspore, and 7% had two aborted

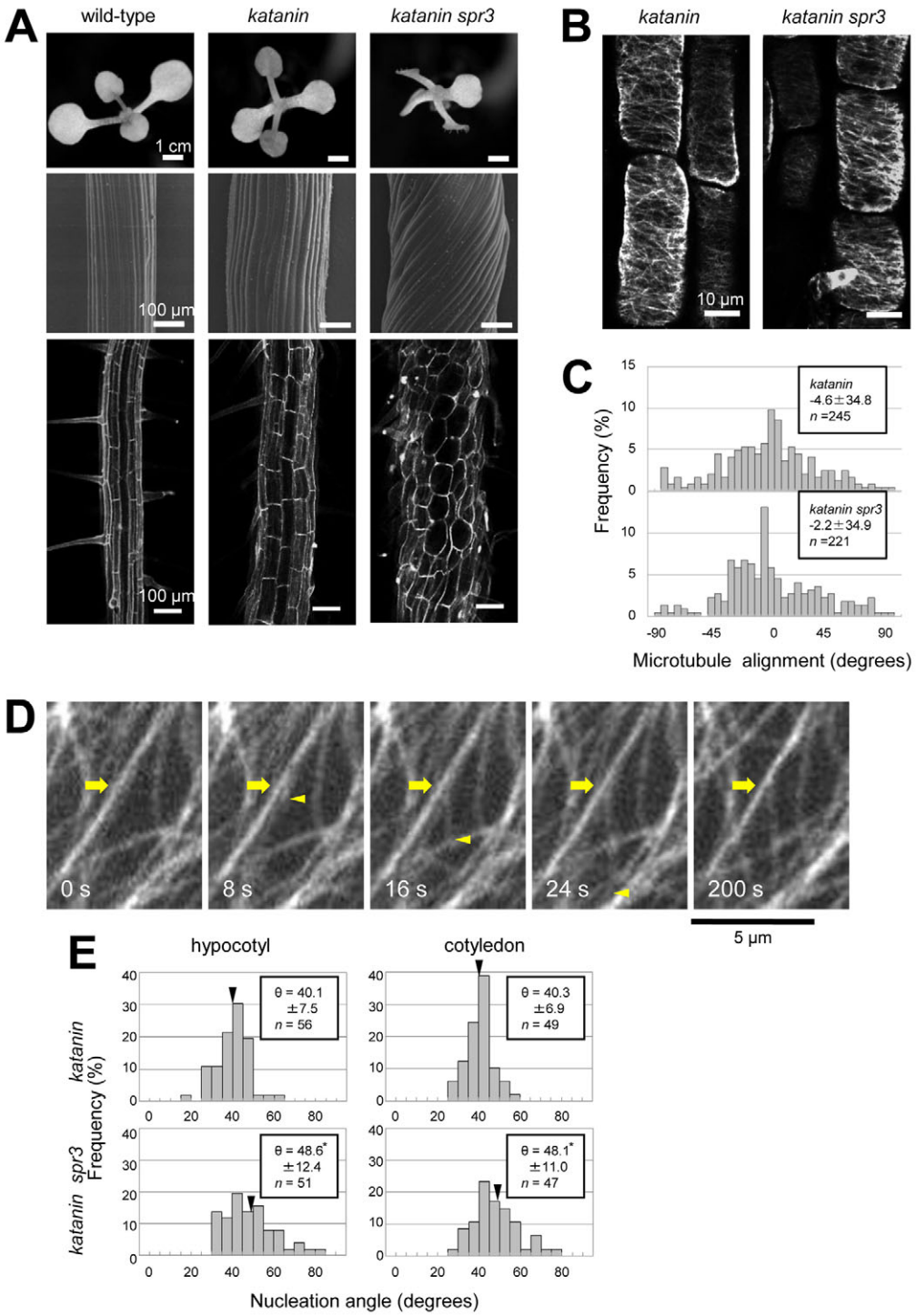

Fig. 5. Morphology and microtubule organization of the *katanin spr3* double mutant. (A) Aerial parts of 10-day-old seedlings (upper panels), etiolated hypocotyls (middle panels) and the differentiated region of primary roots (lower panels) in the wild type, *katanin* mutant and *katanin spr3* double mutant. See the legend to Fig. 1 for imaging techniques. (B) Confocal micrographs of cortical microtubules (labeled with α-tubulin antibodies) at the elongation zone in primary roots. (C) Frequency distribution histograms of microtubule orientations as shown in B. (D) A cortical microtubule (its plus-end indicated with arrowheads) nucleated on a microtubule bundle remains attached to the nucleation site (arrows) even after 200 seconds in a *katanin* mutant cell. We did not observe any release of the minus-end of newly formed microtubules (*n*=47) during the 200-second time interval. By contrast, 35 out of 54 nascent microtubules were released from the nucleation sites within 200 seconds in the control cells. (E) Frequency distribution of microtubule-nucleating angles in cotyledon pavement cells and hypocotyl epidermal cells of *katanin* and *katanin spr3* plants. See the legend of Fig. 1 for details.

microspores (Fig. 6D,E). These results show that GCP2 is required for normal development of both male and female gametophytes.

Discussion

GCP2 is essential for embryogenesis and gametophyte development

As expected from the essential role of the γ-tubulin core complex in microtubule nucleation, *Drosophila* GCP2 mutants die early, during the first and second instars (Colombié et al., 2006). The deletion of GCP2 orthologs in budding and fission yeasts is also lethal (Knop et al., 1997; Vardy and Toda, 2000). In this study, we showed that a T-DNA insertion null allele of *GCP2*, *gcp2-1*, does not produce viable homozygous mutant seeds, and the formation and function of *gcp2-1* gametophytes, especially embryo sac development, were drastically affected. These mutational studies in various organisms thus suggest that the conserved GCP2 subunit of the γ-tubulin core complex is essential for the survival of various organisms, including plants.

In *Arabidopsis*, the simultaneous disruption of two γ-tubulin genes generates aberrant microtubule structures and severely impairs

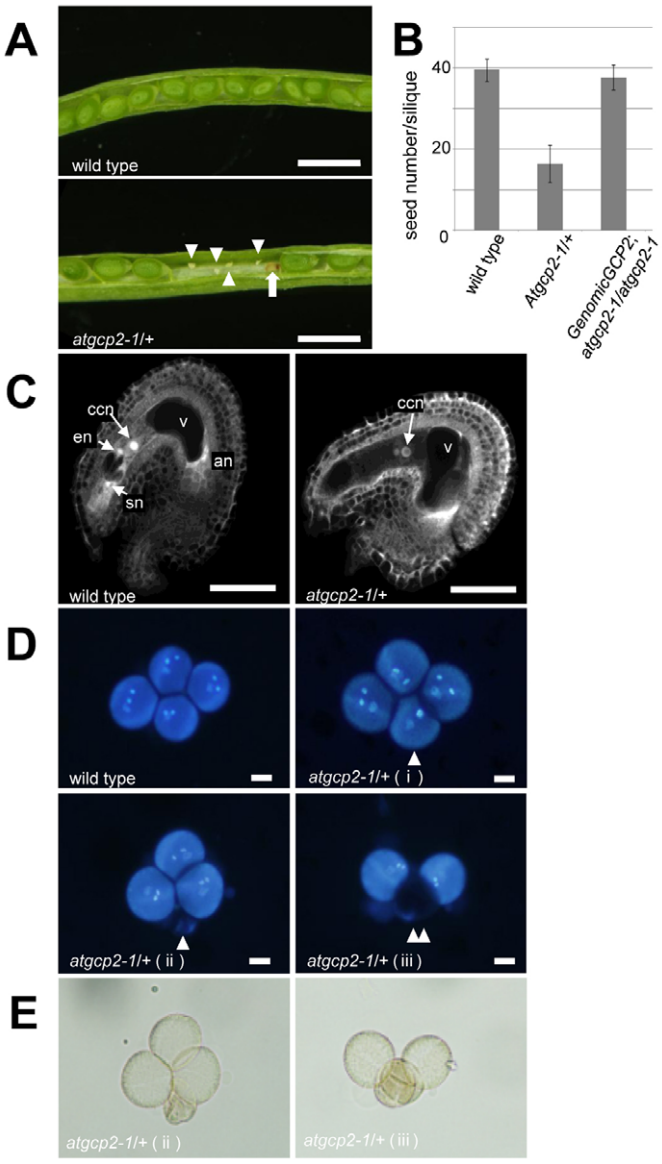

Fig. 6. T-DNA insertion allele of *GCP2* displays gametophytic defects. (A) Siliques of *gcp2-1* heterozygous plants contained normally developed seeds, as well as small aborted seeds (arrow) and presumably unfertilized ovules (arrowheads). (B) Quantification of seeds produced in the siliques of wild-type plants, heterozygous *gcp2-1* plants and homozygous *gcp2-1* plants that had been transformed with the wild-type genomic region of *GCP2*. (C) Confocal microscopic images of female gametophytes. The ovules exhibit autofluorescence with nuclei appearing bright. High percentages of ovules in *gcp2-1*/+ plants contained either two nuclei or one nucleus (now shown) and an aberrant vacant space in the micropylar region, whereas wild-type female gametophytes were composed of a central cell nucleus, an egg nucleus and two synergids nucleoli. v, central vacuole; ccn, central cell nucleus; en, egg nucleolus; sn, synergid nucleoli. (D) Meiotic tetrads in the *qrt* background. A wild-type tetrad and tetrads derived from *gcp2-1*/+ plants, in which bicellular pollen grains (i), one-dead microspores (ii) and two-dead microspores (iii) were observed (arrowheads). (E) Bright-field images of *atgcp2-1*/+ (ii) (left) and *atgcp2-1*/+ (iii) (right) shown in D. Scale bars: 1 mm (A), 50 µm (C) and 10 µm (D).

cell division in gametophytes; >90% of the female gametophytes and >60% of the male gametophytes are non-functional (Pastuglia et al., 2006). These effects of γ-tubulin mutations on gametes are strikingly similar to those of *gcp2-1*, which reflects that these mutations target different components of the same complex. As discussed previously (Pastuglia et al., 2006), a pool of γ-tubulin (and GCP2) might be carried over from parental sporocytes into the gametophytes, and might sustain cell division until the cellular concentration reaches a critical level. This might explain the phenotypic variation seen in the developmental defects in mutant gametophytes (e.g. Fig. 6). The female gametophyte is more severely affected than the male gametophyte, possibly because development of the embryo sac involves three successive mitoses and a larger cellular volume.

A weak *spr3* allele of GCP2 reveals its role in microtubule-dependent microtubule nucleation

The structure of the *Saccharomyces cerevisiae* γ-TuSC was recently analyzed by electron microscopy (resolution, 25 Å), γ-tubulin gold labeling and in vivo FRET (Kollman et al., 2008). In the proposed model, the complex is Y-shaped, with an elongated body (corresponding to the N-termini of Spc97p and Spc98p, the yeast homologs of GCP2 and GCP3) connected to two arms (corresponding to the C-termini of Spc97p and Spc98p, each bound to one molecule of γ-tubulin). The G305R *spr3* mutation in the grip1 motif of GCP2 appears to be located near the neck region at the end of the dimerized body part, although precise placement is not possible at this level of resolution. Our yeast interaction assay also suggests that the G305R mutation compromises interaction between GCP2 and GCP3. That MT nucleation frequency is not significantly affected in the *spr3* cells implies that the mutant GCP2 is incorporated into γ-TuSC and its interaction with GCP3 is perhaps partly stabilized in vivo by other interacting subunits in γ-TuSC or a larger complex.

We observed mild defects in the microtubule dynamics of cortical microtubules; a slight decrease in the growth rate at the plus-end, and a slight increase in rescue frequency at the minus-end. In a partial loss-of-function mutant of the fission yeast GCP2 homolog, the plus ends of interphase and spindle microtubules exhibited abnormal behavior, including cycles of growth and breakage, and hyperstability (Zimmerman and Chang, 2005). Abnormally long microtubules or alterations in microtubule dynamics have also been reported when γ-tubulin, or the homologs of GCP2 and other γ-tubulin complex subunits, are mutated or depleted in yeasts and *Drosophila* (Colombié et al., 2006) (reviewed by Raynaud-Messina and Merdes, 2007). It is quite possible that defective microtubule nucleation increases the cytoplasmic pool of free tubulins, which consequently causes altered microtubule dynamics and an abnormal microtubule structure. Alternatively, the function of the microtubule ends might be directly affected by the microtubule-nucleation complex. In vitro reconstitution experiments suggest that the γ-tubulin ring complex can act as a minus-end-capping protein, by binding directly to the minus-end and preventing microtubule depolymerization (Wiese and Zheng, 2000). A hypothetical model has been postulated, in which a small number of γ-tubulin complexes incorporate into the plus-end microtubule sheets during their closure into polymerizing tubes (Raynaud-Messina and Merdes, 2007).

A striking feature of the *spr3* mutation is its effect on the distribution of microtubule-nucleating angles. In wild-type cells of *Arabidopsis* and tobacco, the angle between the mother microtubule and the newly formed daughter microtubule is well defined with an average value of approximately 40° (Murata et al., 2005) (and this study). The *spr3* mutation of GCP2 relaxes the narrow distribution of the branching angle, and shifts the average to a slightly increased value. The branching points have been shown to contain γ-tubulin

(Murata et al., 2005), and might also contain GCP2 in the form of γ-TuSC or a larger complex. The compromised distribution pattern of the branching angle in *spr3* suggests that GCP2 has an important role in defining the precise physical interaction between the postulated γ-tubulin-containing nucleation complex and a pre-existing mother microtubule. Recent structural analysis revealed how the actin-related protein 2/3 (Arp2/3) complex docks onto a pre-existing mother actin filament to form a new filament at a characteristic ~70° angle (Rouiller et al., 2008). In the actin branch, the Arp2 and Arp3 subunits form a short pitch helix dimer and together contribute the first two subunits of the daughter actin filament. Moreover, all seven subunits of the Arp2/3 complex make some contact with the mother filament. It will be a future challenge to elucidate how an activated γ-tubulin-containing nucleating complex recognizes the side of a mother microtubule in higher plant cells.

Right-handed helical growth and microtubule nucleation

Previous analyses of *Arabidopsis* twisting mutants suggested a correlation between the generation of helical microtubule arrays and the dynamics of individual microtubules (Ishida et al., 2007a). The alteration of microtubule dynamics in the *spr3* cells was not great but could be observed at both ends. However, the helical growth phenotype of the *katanin spr3* double mutant, in which the minus-end of daughter microtubules remained attached to the side of mother microtubules, indicates that the observed minus-end dynamics is not essential for generating twisted growth. We here propose three models that might underlie the mutant array organization.

When a growing plus-end of cortical microtubule encounters a pre-existing microtubule, possible outcomes are influenced by the collision angle. Encounters at angles over ~40° mostly result in crossover or depolymerization, whereas at angles below ~40°, the formation of bundles, where the incoming microtubule is captured and grows in parallel to the encountered microtubule, is favored (Dixit and Cyr, 2004; Ehrhardt, 2008). The critical collision angle of ~40° is intriguingly similar to the nucleation angle of the wild-type cells. The divergent nucleation and convergent capture of nascent microtubules are proposed to be important to maintain the transverse array of cortical microtubules (Murata et al., 2005). When the nucleating angles become more divergent and steeper, as in the *spr3* cells, the intricate balance of collision consequences might be affected. We indeed observed that the microtubule-microtubule encounters in the *spr3* cells result in an increased frequency of depolymerization at the plus-end of incoming microtubules (supplementary material Table S1). Therefore, abnormal microtubule nucleating angles may affect the establishment and maintenance of the transverse array organization.

Alternatively, the altered encounter outcomes as discussed above might result from the slight decrease in the growth rate at the plus end of *spr3* microtubules, and might be independent on the encounter angles. For example, it was recently shown that *Arabidopsis* mutants lacking the CLASP microtubule-associated protein have increased encounter frequencies and are more prone to form bundles at greater encounter angles even though plus-end dynamics do not appear to be distinct from that in the wild type (Ambrose and Wasteneys, 2008).

Finally, γ-tubulin-containing nucleation complexes might be important for generating unskewed cortical microtubules. Microtubules assembled in vitro from pure tubulin dimers are composed of varying numbers of protofilaments (from 12 to 17), in which 14 protofilament microtubules dominate (Wade and Chrétien, 1990; Chrétien and Wade, 1991), whereas in vivo in most cell types, including those of plants, microtubules mostly consist of 13 protofilaments (e.g. Ishida et al., 2007a). Only in the 13-protofilament microtubules, do the protofilaments align strictly parallel to the axis of the microtubule. The protofilaments in the 14 protofilament microtubules, for example, are skewed and form left-handed helices along the microtubule axis. One important function of the γ-tubulin-containing complexes might be to provide a nucleation template to ensure the assembly of 13-protofilament microtubules. In the *spr3* cells with impaired γ-TuSC, the otherwise tight control of the protofilament number might be compromised, resulting in a microtubule population containing some skewed microtubules. Such skewed microtubules might serve as a chirality determinant, which should persist even after individual microtubules are assembled into higher-order bundles (Ishida et al., 2007b). The development of efficient techniques to visualize the protofilament ultrastructure of plant microtubules in vivo (Bouchet-Marquis et al., 2007) is highly anticipated.

Materials and Methods

Plant materials and growth conditions

All the *Arabidopsis thaliana* plants used in this study were of the Wassilewskija ecotype. *gcp2-1* was obtained from INRA (Versailles, France). *spr3* and *katanin* mutants were isolated from seeds mutagenized with ethylmethane sulfonate (Lehle Seeds, Round Rock, TX). The *katanin* allele had a one-base insertion after the 54th base T of the fourth exon, which resulted in the creation of a stop codon at amino acid position 295. A GFP-TUB6-expressing line was generated in the Wassilewskija background, by using the same plasmid reported previously (Nakamura et al., 2004). Plants were grown as described (Furutani et al., 2000).

Map-based cloning

F2 progenies from a cross between *spr3* (Wassilewskija ecotype) and the wild type (Columbia ecotype) were used as a mapping population. The *SPR3* locus was mapped by using DNA markers that were available from The Arabidopsis Information Resource database (http://www.arabidopsis.org) or were newly developed (supplementary material Fig. S1). The two markers closest to the SPR3 locus (marker names based on the resident BAC clone, primer sequences, and restriction enzymes used) are T10B6 (5′-TGAACCGAGTCCATTTACAGA-3′, 5′-TGAGACCTACG-CAACCTTGT-3′ and *Alu*I) and K3M16 (5′-GCGAGTAGAAAGAAGATTT-TGTTGATC-3′, 5′-CAACTAGGAAACTAAATGACATAACCCA-3′ and *Hin*fI). Use of these markers confined the *SPR3* locus to a 30-kb segment on chromosome 5. Seven open reading frames predicted in this region were amplified by PCR from the *spr3* genome and sequenced.

Transgenic plants

The isolation and manipulation of DNA were performed by using standard molecular techniques. A *SPR3* genomic region, which contained a 1058-bp region 5′ upstream of the initiation ATG, all exons and introns, and a 1908-bp region 3′ downstream of the stop codon, was subcloned from a BAC clone T10B6 into pDONR221 by PCR and BP reactions, and then transferred to a Gateway binary vector pGWB1 (Nakagawa et al., 2007) by an LR reaction. The resulting binary vector was introduced into *Agrobacterium tumefaciens* strain MP90 and used to transform *spr3* and *atgcp2-1*/+ plants by the floral dip method (Clough and Bent, 1998). To confirm complement tests, glufosinate (BASTA) resistance in the *atgcp2-1* mutant plants were used.

Immunostaining of microtubules

Microtubules of 4- or 5-day-old seedlings were immunostained, essentially as described by Abe and Hashimoto (Abe and Hashimoto, 2005). Anti-α-tubulin antibody YL1/2 (Abcam, Cambridge, UK) and Alexa Fluor 568-conjugated anti-rat IgG (Molecular Probes, Eugene, OR) were used as primary and secondary antibodies, respectively. Root epidermal cells were observed with a C1 ECLIPSE E600 confocal laser-scanning microscope (Nikon, Tokyo, Japan).

Anatomical imaging of *Arabidopsis* gametophytes

Female gametophyte development was analyzed according to the method of Christensen et al. (Christensen et al., 1997). The 488-nm argon laser of a Nikon C1 confocal microscope was used to illuminate female gametophytes. To analyze male gametophytes, anthers containing mature pollen were brushed on a microscope slide. After staining with DAPI (0.1% Nonidet P-40, 10% DMSO, 50 mM PIPES, pH 7.2, 5 mM EGTA, pH 7.5, and 5 μg/ml DAPI) (Schnurr et al., 2006), pollen grains were covered with a coverslip and observed by using a mercury lamp and a Nikon ECLIPSE E1000 microscope.

Image analysis of microtubule dynamics

Four-day-old seedlings expressing GFP-TUB6 were used for the analysis of microtubule dynamics and nucleating angles in the epidermal cells of upper hypocotyls and in pavement cells of cotyledons. We used a DMRE microscope (Leica, Allendale, NJ) equipped with a CSU10 scanning head (Yokogawa, Tokyo, Japan), a 488-nm argon ion laser (Omnicrome, CA), and an ORCA-ERCCD camera (Hamamatsu Photonics, Shizuoka, Japan). Images were taken every 4 seconds during the course of 4 or 6 minutes at 23°C. Only microtubules for which both leading and lagging ends were visible were analyzed. Dynamic instability parameters were obtained as we described previously (Nakamura et al., 2004). Acquired images were processed and analyzed by using Scion Image (http://www.scioncorp.com/) and ImageJ version 1.40 (http://rsb.info.nih.gov/ij).

We thank Tsuyoshi Nakagawa for pGWB1, Mika Yoshimura and Yugo Komiya for technical assistance, and Takehide Kato for discussion. The SALK Institute Genomic Analysis Laboratory, the Institut National de la Recherche Agronomique, and the Arabidopsis Biological Resource Center are acknowledged for providing the T-DNA knockout alleles and the genomic clones. The work was partly supported by a grant (no. 20370023) and Global COE Program in NAIST (Frontier Biosciences: strategies for survival and adaptation in a changing global environment), MEXT, Japan, and by Ground-based Research for Space Utilization promoted by Japan Space Forum, to T.H. M.N. was supported by a JSPS Research Fellowship for Young Scientists.

References

Abe, T. and Hashimoto, T. (2005). Altered microtubule dynamics by expression of modified α-tubulin protein causes right-handed helical growth in transgenic *Arabidopsis plants*. *Plant J.* **43**, 191-204.

Abe, T., Thitamadee, S. and Hashimoto, T. (2004). Microtubule defects and cell morphogenesis in the *lefty1lefty2* tubulin mutant of *Arabidopsis thaliana*. *Plant Cell Physiol.* **45**, 211-220.

Ambrose, J. C. and Wasteneys, G. O. (2008). CLASP modulates microtubule-cortex interaction during self-organization of acentrosomal microtubules. *Mol. Biol. Cell* **19**, 4730-4737.

Bichet, A., Desnos, T., Turner, S., Grandjean, O. and Höfte, H. (2001). *BOTERO1* is required for normal orientation of cortical microtubules and anisotropic cell expansion in *Arabidopsis*. *Plant J.* **25**, 137-148.

Binarová, P., Cenklová, V., Procházková, J., Doskocilová, A., Volc, J., Vrlik, M. and Bögre, L. (2006). γ-tubulin is essential for acentrosomal microtubule nucleation and coordination of late mitotic events in *Arabidopsis*. *Plant Cell* **18**, 1199-1212.

Bouchet-Marquis, C., Zuber, B., Glynn, A., Eltsov, M., Grabenbauer, M., Goldie, K. N., Thomas, D., Frangakis, A. S., Dubochet, J. and Chrétien, D. (2007). Visualization of cell microtubules in their native state. *Biol. Cell* **99**, 45-53.

Bouquin, T., Mattsson, O., Næsted, H., Foster, R. and Mundy, J. (2003). The *Arabidopsis lue1* mutant defines a katanin p60 ortholog involved in hormonal control of microtubule orientation during cell growth. *J. Cell Sci.* **116**, 791-801.

Burk, D. H. and Ye, Z. (2002). Alteration of oriented deposition of cellulose microfibrils by mutation of a katanin-like microtubule-severing protein. *Plant Cell* **14**, 1-16.

Burk, D. H., Liu, B., Zhong, R., Morrison, W. H. and Ye, Z. (2001). A katanin-like protein regulates normal cell wall biosynthesis and cell elongation. *Plant Cell* **13**, 807-827.

Chan, J., Calder, G. M., Doonan, J. H. and Lloyd, C. W. (2003). EB1 reveals mobile microtubule nucleation sites in *Arabidopsis*. *Nat. Cell Biol.* **5**, 967-971.

Chrétien, D. and Wade, R. H. (1991). New data on the microtubule surface lattice. *Biol. Cell* **71**, 161-174.

Christensen, C. A., King, E. J., Jordan, J. R. and Drews, G. N. (1997). Megagametogenesis in *Arabidopsis* wild type and the Gf mutant. *Sex. Plant Reprod.* **10**, 49-64.

Clough, S. J. and Bent, A. F. (1998). Floral dip: a simplified method for *Agrobacterium* mediated transformation of *Arabidopsis thaliana*. *Plant J.* **16**, 735-743.

Colombié, N., Vérollet, C., Sampaio, P., Moisand, A., Sunkel, C., Bourbon, H., Wright, M. and Raynaud-Messina, B. (2006). The *Drosophila* γ-tubulin small complex subunit Dgrip84 is required for structural and functional integrity of the spindle apparatus. *Mol. Biol. Cell* **17**, 272-282.

Dixit, R. and Cyr, R. (2004). Encounters between dynamic cortical microtubules promote ordering of the cortical array through angle-dependent modifications of microtubule behavior. *Plant Cell* **16**, 3274-3284.

Ehrhardt, D. W. (2008). Straighten up and fly right: microtubule dynamics and organization of non-centrosomal arrays of higher plants. *Curr. Opin. Cell Biol.* **20**, 107-116.

Ehrhardt, D. W. and Shaw, S. L. (2006). Microtubule dynamics and organization of the plant cortical array. *Annu. Rev. Plant Biol.* **57**, 859-875.

Erhardt, M., Stoppin-Mellet, V., Campagne, S., Canaday, J., Mutterer, J., Fabian, T., Sauter, M., Muller, T., Peter, C., Lambert, A. et al. (2002). The plant spc98p homologue colocalizes with γ-tubulin at microtubule nucleation sites and is required for microtubule nucleation. *J. Cell Sci.* **115**, 2423-2431.

Fu, Y., Li, H. and Yang, Z. (2002). The ROP2 GTPase controls the formation of cortical fine F-actin and the early phase of directional cell expansion during *Arabidopsis* organogenesis. *Plant Cell* **14**, 777-794.

Furutani, I., Watanabe, Y., Prieto, R., Masukawa, M., Suzuki, K., Naoi, K., Thitamadee, S., Shikanai, T. and Hashimoto, T. (2000). The *SPIRAL* genes are required for directional control of cell elongation in *Arabidopsis thaliana*. *Development* **127**, 4443-4453.

Gunawardane, R. N., Martin, O. C., Cao, K., Zhang, K., Dej, K., Iwamatsu, A. and Zheng, Y. (2000). Characterization and reconstitution of *Drosophila* γ-tubulin ring complex subunits. *J. Cell Biol.* **151**, 1513-1524.

Ishida, T., Kaneko, Y., Iwano, M. and Hashimoto, T. (2007a). Helical microtubule arrays in a collection of twisting tubulin mutants of *Arabidopsis thaliana*. *Proc. Natl. Acad. Sci. USA* **104**, 8544-8549.

Ishida, T., Thitamadee, S. and Hashimoto, T. (2007b). Twisted growth and organization of cortical microtubules. *J. Plant Res.* **120**, 61-70.

Knop, M., Pereira, G., Geissler, S., Grein, K. and Schiebel, E. (1997). The spindle pole body component Spc97p interacts with the γ-tubulin of *Saccharomyces cerevisias* and functions in microtubule organization and spindle pole body duplication. *EMBO J.* **16**, 1550-1564.

Kollman, J., Zelter, A., Muller, E. G. D., Fox, B., Rice, L. M., Davis, T. N. and Agard, D. A. (2008). The structure of the γ-tubulin small complex: implications of its architecture and flexibility for microtubule nucleation. *Mol. Biol. Cell* **19**, 207-215.

Korolev, A., Buschmann, H., Doonan, J. H. and Lloyd, C. W. (2007). AtMAP70-5, a divergent member of the MAP70 family of microtubule-associated proteins, is required for anisotropic cell growth in *Arabidopsis*. *J. Cell Sci.* **120**, 2241-2247.

Le J., Malley, E. L., Zhang, C., Brankle, S. and Szymanski, D. B. (2006). *Arabidopsis* BRICK1/HSPC300 is an essential WAVE-complex subunit that selectively stabilizes the Arp2/3 activator SCAR2. *Curr. Biol.* **16**, 895-901.

Lucas, J. and Shaw, S. L. (2008). Cortical microtubule arrays in the Arabidopsis seedling. *Curr. Opin. Plant Biol.* **11**, 94-98.

Mathur, J. and Chua, N. (2000). Microtubule stabilization leads to growth reorientation in Arabidopsis trichomes. *Plant Cell* **12**, 465-478.

McNally, F. J. and Vale, R. D. (1993). Identification of katanin, an ATPase that severs and disassembles stable microtubules. *Cell* **75**, 419-429.

Murata, T., Sonobe, S., Baskin, T. I., Hyodo, S., Hasewawa, S., Nagata, T., Horio, T. and Hasebe, M. (2005). Microtubule-dependent microtubule nucleation based on recruitment of γ-tubulin in higher plants. *Nat. Cell Biol.* **7**, 961-968.

Nakagawa, T., Kurose, T., Hino, T., Tanaka, K., Kawamukai, M., Niwa, Y., Toyooka, K., Matsuoka, K., Jinbo, T. and Kimura, T. (2007). Development of series of gateway binary vectors, pGWBs, for realizing efficient construction of fusion genes for plant transformation. *J. Biosci. Bioeng.* **104**, 34-41.

Nakamura, M., Naoi, K., Shoji, T. and Hashimoto, T. (2004). Low concentrations of propyzamide and oryzalin alter microtubule dynamics in *Arabidopsis* epidermal cells. *Plant Cell Physiol.* **45**, 1330-1334.

Paradez, A., Wright, A. and Ehrhardt, D. W. (2006). Microtubule cortical array organization and plant cell morphogenesis. *Curr. Opin. Plant Biol.* **9**, 571-578.

Pastuglia, M. and Bouchez, D. (2007). Molecular encounters at microtubule ends in the plant cell cortex. *Curr. Opin. Plant Biol.* **10**, 557-563.

Pastuglia, M., Azimzadeh, J., Goussot, M., Camilleri, C., Belcram, K., Evrard, J., Schmit, A., Guerche, P. and Bouchez, D. (2006). γ-tubulin is essential for microtubule organization and development in *Arabidopsis*. *Plant Cell* **18**, 1412-1425.

Perrin, R. M., Wang, Y., Yuen, C. Y. L., Will, J. and Masson, P. H. (2007). WVD2 is a novel microtubule-associated protein in *Arabidopsis thaliana*. *Plant J.* **49**, 961-971.

Preuss, D., Rhee, S. Y. and Davis, R. W. (1994). Tetrad analysis possible in Arabidopsis with mutation of the QUARTET (QRT) genes. *Science* **264**, 1458-1460.

Raynaud-Messina, B. and Merdes, A. (2007). γ-tubulin complexes and microtubule organization. *Curr. Opin. Cell Biol.* **19**, 24-30.

Rouiller, I., Xu, X., Amann, K. J., Egile, C., Nickell, S., Nicastro, D., Li, R., Pollard, T. D., Volkmann, N. and Hanein, D. (2008). The structural basis of actin filament branching by the Arp2/3 complex. *J. Cell Biol.* **180**, 887-895.

Schnurr, J. A., Storey, K. K., Jung, H. G., Somers, D. A. and Gronwald, J. W. (2006). UDP-sugar pyrophosphorylase is essential for pollen development in Arabidopsis. *Planta* **224**, 520-532.

Seltzer, V., Janski, N., Canaday, J., Herzog, E., Erhardt, M., Evrard, J. and Schmit, A. (2007). Arabidopsis GCP2 and GCP3 are part of a soluble γ-tubulin complex and have nuclear envelope targeting domains. *Plant J.* **52**, 322-331.

Shaw, S. L., Kamyar, R. and Ehrhardt, D. W. (2003). Sustained microtubule treadmilling in *Arabidopsis* cortical arrays. *Science* **300**, 1715-1718.

Shimamura, M., Brown, R. C., Lemmon, B. E., Akashi, T., Mizuno, K., Nishihara, N., Tomizawa, K., Yoshimoto, K., Deguchi, H., Hosoya, H. et al. (2004). γ-tubulin in land plants: characterization, localization, and implication in the evolution of acentriolar microtubule organizing centers. *Plant Cell* **16**, 45-59.

Vardy, L. and Toda, T. (2000). The fission yeast γ-tubulin complex is required in G_1 phase and is a component of the spindle assembly checkpoint. *EMBO J.* **19**, 6098-6111.

Wade, R. H. and Chrétien, D. (1990). Characterization of microtubule protofilament numbers: how does the surface lattice accommodate? *J. Mol. Biol.* **212**, 775-786.

Wasteneys, G. O. (2002). Microtubule organization in the green kingdom: chaos or self-order? *J. Cell Sci.* **115**, 1345-1354.

Wasteneys, G. O. and Williamson, R. E. (1989). Reassembly of microtubules in *Nitella tasmanica*: assembly of cortical microtubules in branching clusters and its relevance to steady-state microtubule assembly. *J. Cell Sci.* **93**, 705-714.

Wiese, C. and Zheng, Y. (2000). A new function for the γ-tubulin ring complex as a microtubule minus-end cap. *Nat. Cell Biol.* **2**, 358-364.

Wiese, C. and Zheng, Y. (2006). Microtubule nucleation: γ-tubulin and beyond. *J. Cell Sci.* **119**, 4143-4153.

Yao, M., Wakamatsu, Y., Itoh, T. J., Shoji, T. and Hashimoto, T. (2008). *Arabidopsis* SPIRAL2 promotes uninterrupted microtubule growth by suppressing the pause state of microtubule dynamics. *J. Cell Sci.* **121**, 2372-2381.

Zimmerman, S. and Chang, F. (2005). Effects of γ-tubulin complex proteins on microtubule nucleation and catastrophe in fission yeast. *Mol. Biol. Cell* **16**, 2719-2733.